Electronic Supplementary Information for

A Straightforward Gradient-Based Approach for Designing Superconductors with High Critical Temperature: Exploiting Domain Knowledge via Adaptive Constraints

Akihiro Fujii*[a], Anh Khoa Augustin Lu[a,b], Koji Shimizu[c], and Satoshi Watanabe[a]

[a] The University of Tokyo, Department of Materials Engineering, Faculty of Engineering Bldg. IV, 7-3-1, Hongo, Bunkyo-ku, Tokyo 113-8656, Japan. E-mail: akihiro.fujii@cello.t.u-tokyo.ac.jp
[b] National Institute for Materials Science (NIMS), 1-1 Namiki, Tsukuba, Ibaraki 305-0044, Japan
[c] National Institute of Advanced Industrial Science and Technology (AIST), 1-1-1 Umezono, Tsukuba, Ibaraki 305-8568, Japan

S.1 T_c prediction model

We trained a deep learning model f_{T_c} to predict the critical temperature (T_c) from composition, utilizing the SuperCon dataset as the source of superconductor data. Konno *et al.*[12] reported that training only on the SuperCon dataset increases false positives (i.e., mistakenly predicting non-superconductors as superconductors), so we added the Crystallography Open Database (COD)[43–51] as a dataset of non-superconductors to training data. We trained the ResNet18 regression model using Adam optimiser [40] with a learning rate of 0.0001 and a batch size of 1024. Given that $T_c \geq 0$, we employed the Rectified Linear Unit (ReLU) as the activation function at the output layer.

S.1.1 Dataset

We used the SuperCon dataset for superconductor materials. For preprocessing, we excluded substances whose compositions were not quantitatively specified, such as those denoted by variables (e.g., x, y, z). We also used the Crystallography Open Database (COD) for the non-superconductor materials. Furthermore, compositions identical to those in the SuperCon data were excluded from the COD data. We employed the SuperCon database (version 220808) and accessed the COD dataset on March 22, 2023.

For both SuperCon and COD, compositions were represented by 118-dimensional (from H to Og) distribution vectors x, normalised to sum to 1. The critical temperature (T_c) was used as the target variable y, setting y=0 for non-superconducting materials from the COD dataset and using the actual T_c values from the SuperCon dataset. For substances with identical compositional ratios but different T_c values, we calculated the mean T_c value. We found that 13.1% of the compositions have duplicate T_c reports. For these compositions, the mean standard deviation per composition of the reported T_c values is 2.2 K. Consequently, we obtained 14,410 data points for the SuperCon dataset and 373,901 data points for the COD dataset. Materials with the same combination of elements may cause data leakage if they are split across different data partitions. Therefore, we ensured that materials with the same combination of elements were placed in the same data partition during the data split. We then randomly split these into training, validation, and test sets in the ratios of 0.80:0.05:0.15, respectively.

However, we were concerned about the model's accuracy due to an imbalance in the training data resulting from a smaller number of superconductors compared to non-superconductors. Therefore, to address this imbalance, we augmented the training data by increasing the number of instances from the SuperCon dataset by a factor of 25 through replication.

S.1.2 Element representation

As element features $\mathbf{a}$, we utilized flag representations for the s, p, d, and f electron orbitals as embedded in the periodic table[12]. Each element i has a feature tensor $\mathbf{a}$ with dimensions of $4\times7\times32$, representing the channels for the s, p, d, and f electron orbitals, periods, and groups. Note that, due to the extension of lanthanides and actinides in the group direction, the third dimension (group) extends to 32, not 18. For any element i, its feature $\mathbf{a}^i$ assigns a value of 1 at the position in the periodic table corresponding to the outermost electron's channel and 0 values for all other positions.

$$\mathbf{A}_i = \mathbf{a}^i, \quad \mathbf{A} \in \{0,1\}^{118\times4\times7\times32}, \quad i \in \{\mathbf{H}, \mathbf{He}, ..., \mathbf{Og}\} \tag{S.1.1}$$

(S.1.2)

$$\mathbf{A}_{ijkl} = \begin{cases} 1 & \text{if atom } i \text{ has its outermost electrons, family (group),} \\ & \text{and period corresponding to } j, k, \text{ and } l. \\ 0 & \text{otherwise} \end{cases} \tag{S.1.3}$$

For instance, the hydrogen atom, which has a 1s electron in its outermost shell and belongs to the first period and group, is represented by the feature $\mathbf{a}^{\mathrm{H}}$. This feature has a value of one at position $(1,1,1)$ and zeroes elsewhere. Similarly, the feature for chlorine, $\mathbf{a}^{\mathrm{Cl}}$, which contains 3p electrons in its outer shell and is located in the third period and seventeenth group, has a

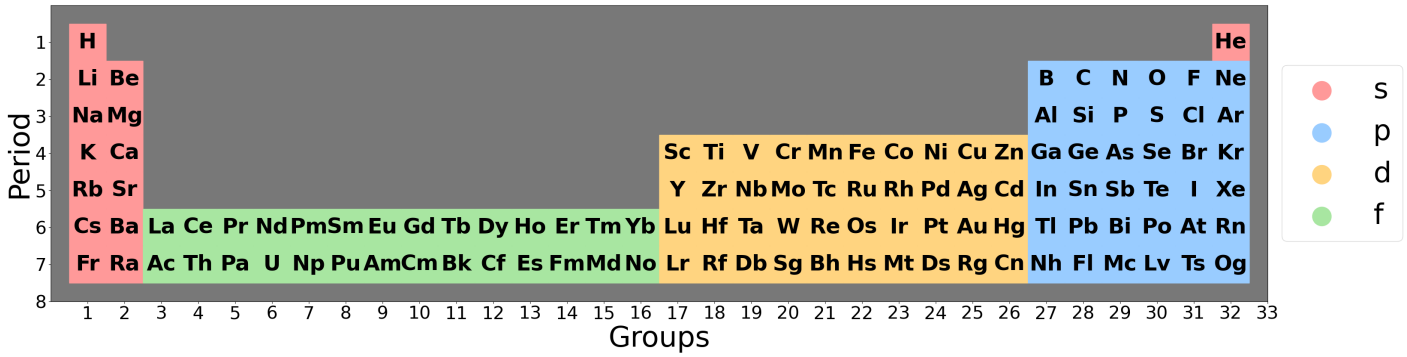

Fig. S.1.1 Periodic table, coloured according to the type of orbital occupied by the outermost electron.

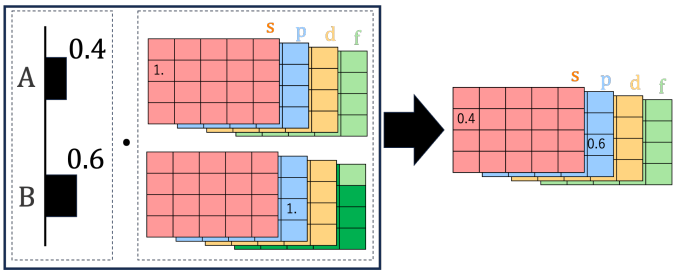

Fig. S.1.2 Example: Representation of the composition A_2B_3

value of 1 at position $(2,3,31)$ and zeros elsewhere. Fig. S.1.1 illustrates the corresponding channel of the outermost electron for each element. The composition's representation is calculated by computing the product of the composition vector and the element features **a**, as shown in Fig. S.1.2.

S.1.3 Prediction scores

Since previous methods were evaluated only on SuperCon data, we first evaluated our model solely on the SuperCon dataset (Table S.1.1). Note that it is not a direct comparison due to differences in data splitting. The previous studies did not describe whether they consider the combination of elements in the data split. We assume that the previous studies did not perform such data splitting. Our model was the only one trained on both SuperCon and COD datasets. Our model demonstrated competitive results compared to other methods when using only SuperCon data. The model trained using COD and considering the combination of elements in the data split scored worse than the model trained only on SuperCon. However, as we will discuss in Section S.1.4, it was found that using COD is important to reduce false positives. Therefore, we adopted this model.

S.1.4 Reducing false positives

Here, we addressed the issue of false positives, that is, non-superconductors incorrectly predicted to be superconductors. Konno *et al.*[12] stated that models trained exclusively on the SuperCon dataset tend to produce a significant number of false positives, although this claim has not been numerically demonstrated. Hence, we numerically assessed how incorporating the COD dataset, which consists of non-superconductors, impacts the rate of false positives.

We performed this assessment using our model, a ResNet18 regression model and adopted the precision score as our metric. The precision score is defined as tp/(tp+fp), where tp (true positive) denotes the probability of accurately predicting a superconductor (y>0) as superconductor (i.e., $f_{T_c}(x) > 0$), and fp (false positive) represents the probability of mistakenly predicting a non-superconductor (y=0) as a superconductor (i.e., $f_{T_c}(x) > 0$).

Table S.1.2 provides a comparison of precision scores between models trained on the SuperCon dataset alone and those trained on both SuperCon and COD datasets. It is evident that models trained with the inclusion of the COD dataset exhibit a significantly higher precision score compared to those trained exclusively on the SuperCon dataset. This outcome underscores the necessity of integrating non-superconductors into the training process for superconductor material design tasks, where non-superconductors might emerge as potential candidates.

S.2 Formation energy prediction model

In this study, we employed ElemNet[52] as the formation energy prediction model. Although its original implementation (`https://github.com/NU-CUCIS/ElemNet`) uses TensorFlow 1.x, we require gradient information in PyTorch. Thus, we re-implemented the model in PyTorch. We follow the same model architecture, training parameters, and dataset usage detailed in Jha *et al.*[52], and the performance of our re-implementation is presented in Table S.2.1.

S.3 SuperDiff and SuperDiff w/ CG

We implemented SuperDiff by following the procedures outlined in its original paper and official implementations. Specifically, we

Table S.1.1 Results on SuperCon data and comparison with other methods.

Method	Train Dataset	Elem Div	MAE	R2
Stanev *et al.*[7]	SuperCon	False?	-	0.88
Zeng *et al.*[9]	SuperCon	False?	4.21	0.97
Dan *et al.*[10]	SuperCon	False?	-	0.907
Taheri *et al.*[14]	SuperCon	False?	-	0.927
Ours	SuperCon	False	4.90	0.92
Ours	SuperCon + COD	True	7.84	0.80

Algorithm 2 SuperDiff using ILVR Sampling Procedures with Classifier Guidance

$x_T \sim \mathcal{N}(\mathbf{0}, \mathbf{I})$
for $t = T, \ldots, 1$ **do**
  $z \sim \mathcal{N}(\mathbf{0}, \mathbf{I})$ if $t > 1$, else $z = 0$
  $x'_{t-1} \leftarrow \frac{1}{\sqrt{\alpha_t}}\left(x_t - \frac{1-\alpha_t}{\sqrt{1-\bar{\alpha}_t}}\epsilon_\theta(x_t, t)\right) + \sigma_t z$ ▷ Denoising
  $x_{t-1} \leftarrow x_{t-1} - w\nabla L(x_{t-1})$ ▷ Guidance with predictors
  $x_{t-1} \leftarrow \phi_N(y_{t-1}) + x'_{t-1} - \phi_N(x'_{t-1})$ ▷ ILVR using sample y
end for
return x_0 ▷ Generated sample

Table S.1.2 Precision scores with respect to the training set.

Training data	Precision score
SuperCon	0.065
SuperCon+COD	**0.804**

Table S.2.1 Comparison of MAE score of ElemNet with the original paper.

Methods	Original[52]	Our replication
MAE (eV/atom)	0.05	0.07

divided the dataset used for training the T_c prediction model into cuprates, pnictides, and others, then trained SuperDiff separately for each category. While the T_c prediction model was trained on normalised compositions, SuperDiff was trained without normalisation.

For conditional inference using Iterative Latent Variable Refinement (ILVR), we selected the appropriate SuperDiff model (cuprates, pnictides, or others) based on the reference material. We then applied guidance through "Classifier Guidance (CG)" using both the T_c prediction model and ElemNet with the loss function described in equation 1. Although neither is strictly a classifier, we refer to this approach as CG for convenience. We describe two inference algorithms: one that performs ILVR-based conditional inference with SuperDiff in Algorithm 1, and one that further incorporates the two prediction models as guidance in Algorithm 2. Note that Algorithm 2 is not proposed in Yuan *et al.*[27].

Normally, the classifier used for CG must be trained on data with added noise, which would make Universal Guidance (UG) the better choice for off-the-shelf models. However, our experiments showed that CG still improved T_c without noise-augmented training. Therefore, we decided to use CG. We hypothesize that the reason CG remained effective despite the absence of noise-augmented training is that our T_c prediction model and formation energy prediction model both take normalised compositions as inputs, thereby reducing the impact of noise.

Algorithm 1 SuperDiff using ILVR Sampling Procedures

$x_T \sim \mathcal{N}(\mathbf{0}, \mathbf{I})$
for $t = T, \ldots, 1$ **do**
  $z \sim \mathcal{N}(\mathbf{0}, \mathbf{I})$ if $t > 1$, else $z = 0$
  $x'_{t-1} = \frac{1}{\sqrt{\alpha_t}}\left(x_t - \frac{1-\alpha_t}{\sqrt{1-\bar{\alpha}_t}}\epsilon_\theta(x_t, t)\right) + \sigma_t z$ ▷ Denoising
  $x_{t-1} = \phi_N(y_{t-1}) + x'_{t-1} - \phi_N(x'_{t-1})$ ▷ ILVR using sample y
end for
return x_0 ▷ Generated sample

Table S.3.1 Total changes in T_c resulting from guidance and denoising during the 1000 steps in SuperDiff w/ CG **without ILVR**. "Guide weight" denotes the weight w used for guidance in Algorithm 2. "Denoise ΔT_c", "ILVR ΔT_c" and "Guide ΔT_c" represent the cumulative change in T_c per step due to denoising, ILVR, or the guidance. "Sum" is the total of these values. "Screening ratio" denotes the ratio of the number of screened samples to the total number of samples.

Guide weight w	Denoise ΔT_c (K)	ILVR ΔT_c (K)	Guide ΔT_c (K)	Sum (K)
-	20.1	-	-	20.1
1.0×10^{-5}	19.6	-	0.6	20.2
1.0×10^{-4}	14.5	-	5.3	19.8
1.0×10^{-3}	-39.0	-	62.1	23.1
1.0×10^{-2}	-558.6	-	620.7	62.1
1.0×10^{-1}	-854.1	-	916.6	62.5
1.0	-9.2	-	31.8	22.5
1.0×10^{1}	-0.1	-	6.8	6.7
1.0×10^{2}	-0.1	-	4.0	3.9

S.3.1 Guidance vs denoise without ILVR

We also repeated the experiments from Table 4 without using ILVR. As shown in Table S.3.1, even without ILVR, excessive increases in T_c are still suppressed by denoising. We hypothesize that properties far from the data distribution are treated as "noise" by the diffusion model and consequently removed.

S.4 Random seed effects in KIAGO optimisation in the first stage

To evaluate the impact of the random seed in KIAGO's initialization—i.e., perturbing known superconductors by randomly substituting elements and adding new elements to the composition—we selected several base materials, generated perturbed compositions, and performed first stage optimization (equations 12 to 14) under five distinct seeds (128 samples per run).

The results are shown in Table S.4.1. Performance varies only slightly across seeds (mean ± standard deviation), indicating that first stage optimization is robust to random initialization and yields consistent improvements irrespective of the seed.

Table S.4.1 Top-30 T_c results from the 500-step first-stage optimisation (mean ± standard deviation), computed over five random seeds with 128 samples each.

base material	Top-30 (K)
$LaPt_2B_2C$	45.6 ± 1.9
$SrFe_{1.88}Ni_{0.12}As_2$	71.9 ± 2.8
LaNiAsO	53.1 ± 3.4
$CeBiS_2O$	29.8 ± 4.7
$Bi_2Sr_2CuO_6$	104.4 ± 2.5
$Sr_4V_2Fe_2As_2O_6$	68.4 ± 5.8
$TlSr_2CaCu_2O_7$	134.2 ± 1.1
$HgBa_2Ca_2Cu_3O_8$	146.7 ± 1.0

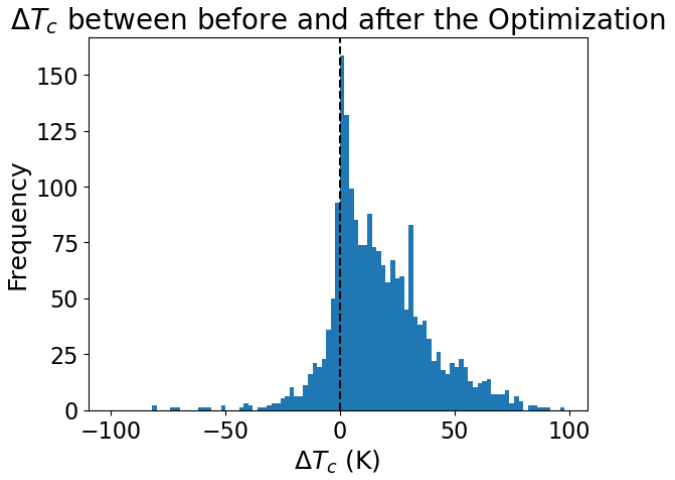

Fig. S.5.1 Changes in T_c due to optimisation.

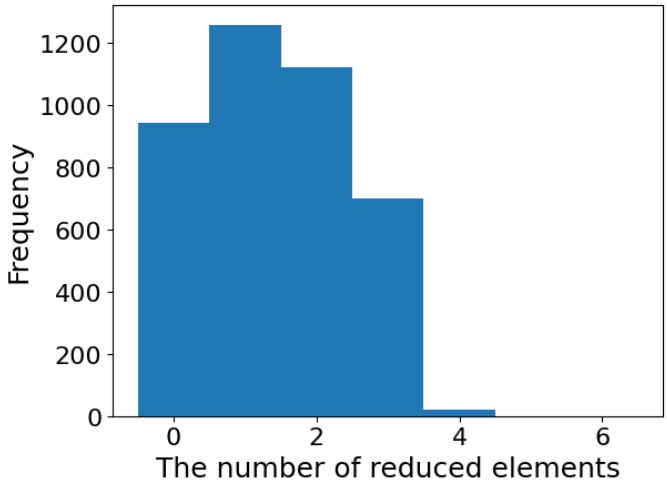

Fig. S.5.2 Change in number of element types due to optimisation (a positive number denotes the number of element type decreases after optimisation).

S.5 KIAGO optimisation in the first stage

Here, we show the results of the optimisation using equations 12 to 14. Fig. S.5.1 shows that most of samples have higher T_c after optimisation. However, some samples have lower T_c after optimisation. This is likely due to the presence of many local minima. Furthermore, we observed a tendency for the number of element types to decrease due to optimisation (Fig. S.5.2).

S.6 Detailed results

Table S.6.1 shows the detailed results of the experiments presented in Table 2 in Section 3.4. Each column in Table S.6.1 represents the fraction that fulfills each screening criterion. The last column shows the difference between the average T_c of the top 30 screened samples and the base materials.

Table S.6.2 shows the detailed results of the experiments presented in Table 5, 6 and 7 in Section 3.5. Each column in Table S.6.2 represents the fraction that fulfills each screening criterion. The last column shows the difference between the average T_c of the top 30 screened samples and the base materials.

Table S.6.1 All results of Screening rates and T_c. "Unique rate" indicates the fraction of unique compositions among the 4,096 samples. "ELM < 10," "Neutrality," "ElecNeg," and "E_f < 0.0 eV" denote, respectively, the percentage of these unique samples that: contain at most 9 elements ("ELM < 10"); satisfy charge neutrality per SMACT ("Neutrality"); meet electronegativity criterion using SMACT ("ElecNeg"); achieve predicted formation energy below 0.0 eV ('E_f < 0.0 eV'). "Screened rate" is the fraction that fulfills all these screening criteria among all 4,096 samples. "ΔT_c Top-30 (K)" represents the difference between the average predicted T_c of the top 30 screened samples and the base materials.

Base materials from SuperCon	Method	Unique rate	ELM < 10	Neutrality	ElecNeg	E_f < 0.0 eV	Screened rate	ΔT_c Top-30 (K)
LaNiAsO	KIAGO	0.98	1.00	0.88	0.77	0.99	0.76	104.39
	SD	1.00	0.50	0.08	0.01	0.96	0.01	-1.42
	SD w/ CG	1.00	0.48	0.09	0.01	0.96	0.01	-0.47
	C-ES	0.89	1.00	0.99	0.85	1.00	0.85	16.43
$SrFe_{1.88}Ni_{0.12}As_2$	KIAGO	0.99	1.00	0.91	0.74	0.71	0.54	97.91
	SD	1.00	0.46	0.05	0.00	0.21	0.00	26.76
	SD w/ CG	1.00	0.50	0.04	0.00	0.87	0.00	4.53
	C-ES	0.50	1.00	0.98	0.73	0.93	0.68	18.75
$Sr_4V_2Fe_2As_2O_6$	KIAGO	0.98	1.00	0.85	0.73	0.98	0.71	97.49
	SD	1.00	0.12	0.29	0.05	0.51	0.01	-13.77
	SD w/ CG	1.00	0.12	0.29	0.05	0.89	0.01	-13.66
	C-ES	0.86	1.00	1.00	0.96	1.00	0.96	0.25
$LaPt_2B_2C$	KIAGO	0.98	1.00	0.83	0.70	0.93	0.68	86.73
	SD	1.00	0.52	0.06	0.01	0.87	0.01	-5.01
	SD w/ CG	1.00	0.58	0.06	0.02	0.84	0.01	-4.66
	C-ES	0.89	1.00	0.71	0.54	0.75	0.40	4.84
$HgBa_2Ca_2Cu_3O_8$	KIAGO	0.74	1.00	0.77	0.67	0.98	0.66	17.07
	SD	1.00	0.57	0.00	0.00	1.00	0.00	-29.43
	SD w/ CG	1.00	0.57	0.00	0.00	1.00	0.00	-1.18
	C-ES	0.88	1.00	0.99	0.97	1.00	0.97	0.59
$CeBiS_2O$	KIAGO	0.97	1.00	0.88	0.79	1.00	0.79	92.12
	SD	1.00	0.21	0.14	0.01	0.23	0.00	N/A
	SD w/ CG	1.00	0.50	0.11	0.01	0.97	0.01	-0.31
	C-ES	0.86	1.00	1.00	0.95	1.00	0.95	2.25
$Bi_2Sr_2CuO_6$	KIAGO	0.89	1.00	0.85	0.68	0.99	0.67	129.63
	SD	1.00	0.76	0.01	0.01	1.00	0.01	18.34
	SD w/ CG	1.00	0.74	0.01	0.01	1.00	0.01	26.76
	C-ES	0.88	1.00	0.99	0.96	1.00	0.96	48.91
$TlSr_2CaCu_2O_7$	KIAGO	0.69	1.00	0.81	0.69	0.98	0.68	76.32
	SD	1.00	0.67	0.01	0.01	1.00	0.00	5.21
	SD w/ CG	1.00	0.68	0.01	0.01	1.00	0.00	12.42
	C-ES	0.86	1.00	0.99	0.96	1.00	0.96	33.16

Table S.6.2 "Keeping remaining atoms" is the percentage of generated compositions in which the designated set of elements and their compositions are preserved within a 1% error (e.g., In the top row of the table, the composition of $FeAsF_{0.2}O_{0.8}$ in $CeFeAsF_{0.2}O_{0.8}$.) "Keeping sum of substitute atoms" is the percentage in which the total substituted composition—excluding the designated elements and compositions—matches the targeted substituted element's composition within 1% error (e.g., In the top row of the table, the composition of Ce^{+3} in $CeFeAsF_{0.2}O_{0.8}$.). Other metrics follow the definitions in Table S.6.1.

Base materials from SuperCon	Substitute target	Method	Unique rate	ELM < 10	Neutrality	ElecNeg	$E_f < 0.0$ eV	Keeping sum of substitute atoms	Keeping remain atoms	Screening rate	ΔT_c Top-30 (K)
$CeFeAsF_{0.2}O_{0.8}$	Ce^{+3}	KIAGO	0.98	1.00	1.00	0.30	1.00	1.00	1.00	0.30	14.17
	Ce^{+3}	SD	1.00	0.40	0.03	0.01	0.54	0.00	0.13	0.00	N/A
	Ce^{+3}	SD w/ CG	1.00	0.37	0.02	0.00	0.85	0.00	0.12	0.00	N/A
	Ce^{+3}	C-ES	0.83	1.00	1.00	0.49	1.00	1.00	1.00	0.49	9.96
LaFeAsO	La^{+3}	KIAGO	0.99	1.00	1.00	0.17	1.00	1.00	1.00	0.17	33.88
	La^{+3}	SD	1.00	0.45	0.02	0.01	0.58	0.04	0.18	0.00	1.24
	La^{+3}	SD w/ CG	1.00	0.39	0.02	0.00	0.86	0.03	0.17	0.00	N/A
	La^{+3}	C-ES	0.84	1.00	1.00	0.47	1.00	1.00	1.00	0.47	31.10
$SrFe_2As_2$	Sr^{+2}	KIAGO	1.00	1.00	1.00	0.32	0.97	1.00	1.00	0.32	31.54
	Sr^{+2}	SD	1.00	0.52	0.03	0.00	0.21	0.04	0.15	0.00	N/A
	Sr^{+2}	SD w/ CG	1.00	0.48	0.05	0.01	0.87	0.04	0.14	0.00	N/A
	Sr^{+2}	C-ES	0.87	1.00	1.00	0.35	0.87	1.00	1.00	0.32	19.25
$Bi_2CaSr_2Cu_2O_8$	Bi^{+3}	KIAGO	0.99	1.00	1.00	1.00	1.00	1.00	1.00	1.00	18.72
	Bi^{+3}	SD	1.00	0.70	0.01	0.01	1.00	0.41	0.56	0.00	0.15
	Bi^{+3}	SD w/ CG	1.00	0.64	0.01	0.01	1.00	0.38	0.53	0.00	-1.11
	Bi^{+3}	C-ES	0.81	1.00	1.00	0.95	1.00	1.00	1.00	0.95	6.10
$CeNiC_2$	Ce^{+4}	KIAGO	0.94	1.00	1.00	0.75	0.50	1.00	1.00	0.50	13.10
	Ce^{+4}	SD	1.00	0.72	0.07	0.03	0.98	0.02	0.04	0.00	N/A
	Ce^{+4}	SD w/ CG	1.00	0.77	0.06	0.03	0.93	0.02	0.05	0.00	-0.02
	Ce^{+4}	C-ES	0.87	1.00	1.00	0.59	0.17	1.00	1.00	0.13	4.33
$LaNiC_2$	La^{+3}	KIAGO	1.00	1.00	1.00	0.90	0.77	1.00	1.00	0.75	10.53
	La^{+3}	SD	1.00	0.76	0.03	0.01	0.98	0.07	0.12	0.00	N/A
	La^{+3}	SD w/ CG	1.00	0.76	0.04	0.01	0.92	0.06	0.11	0.00	N/A
	La^{+3}	C-ES	0.87	1.00	1.00	0.72	0.35	1.00	1.00	0.28	4.90
$MgCoNi_3$	Co^{+2}	KIAGO	1.00	1.00	1.00	0.93	1.00	1.00	1.00	0.93	31.66
	Co^{+2}	SD	1.00	0.42	0.71	0.65	0.36	0.01	0.02	0.00	N/A
	Co^{+2}	SD w/ CG	1.00	0.16	0.63	0.51	0.63	0.01	0.02	0.00	0.13
	Co^{+2}	C-ES	0.87	1.00	1.00	0.40	0.99	1.00	1.00	0.40	7.23
$RuSr_2GdCu_2O_8$	Sr^{+2}	KIAGO	0.54	1.00	1.00	1.00	1.00	1.00	1.00	1.00	-3.38
	Sr^{+2}	SD	1.00	0.55	0.05	0.04	1.00	0.13	0.21	0.00	-0.23
	Sr^{+2}	SD w/ CG	1.00	0.55	0.06	0.05	1.00	0.13	0.21	0.00	-0.16
	Sr^{+2}	C-ES	0.81	1.00	1.00	0.95	1.00	1.00	1.00	0.95	5.64
$RuSr_2YCu_2O_8$	Y^{+3}	KIAGO	0.97	1.00	1.00	1.00	1.00	1.00	1.00	1.00	45.96
	Y^{+3}	SD	1.00	0.65	0.08	0.06	1.00	0.09	0.29	0.00	-0.89
	Y^{+3}	SD w/ CG	1.00	0.63	0.07	0.06	1.00	0.11	0.28	0.00	1.53
	Y^{+3}	C-ES	0.81	1.00	1.00	0.95	1.00	1.00	1.00	0.95	37.74
$Y_2Fe_3Si_5$	Y^{+3}	KIAGO	1.00	1.00	1.00	0.56	1.00	1.00	1.00	0.56	5.57
	Y^{+3}	SD	1.00	0.33	0.18	0.05	0.56	0.03	0.05	0.00	N/A
	Y^{+3}	SD w/ CG	1.00	0.23	0.26	0.08	0.87	0.02	0.03	0.00	N/A
	Y^{+3}	C-ES	0.88	1.00	1.00	0.19	0.98	1.00	1.00	0.18	1.50
YIrSi	Y^{+3}	KIAGO	1.00	1.00	1.00	0.12	1.00	1.00	1.00	0.12	6.09
	Y^{+3}	SD	1.00	0.90	0.28	0.06	0.70	0.02	0.04	0.00	3.42
	Y^{+3}	SD w/ CG	1.00	0.55	0.48	0.07	0.92	0.02	0.03	0.00	N/A
	Y^{+3}	C-ES	0.88	1.00	1.00	0.39	0.99	1.00	1.00	0.38	3.86